Title
Silver Diamine Fluoride Differentially Affects Dentin and Hypomineralized Enamel Permeabilities

Author
Chou, Conrad

Publication Date
2023

Peer reviewed|Thesis/dissertation

Silver Diamine Fluoride Differentially Affects Dentin and Hypomineralized Enamel Permeabilities

by
Conrad Chou

THESIS
Submitted in partial satisfaction of the requirements for degree of
MASTER OF SCIENCE

in

Oral and Craniofacial Sciences

in the

GRADUATE DIVISION
of the
UNIVERSITY OF CALIFORNIA, SAN FRANCISCO

Approved:

DocuSigned by:
Dr. Sunita Ho
B3DEF15BD3D8415...

Dr. Sunita Ho
Chair

DocuSigned by:
Thomas Tanbonliong
DocuSigned by:

Thomas Tanbonliong

DocuSigned by:
Thuan Le
DocuSigned by:

Thuan Le

DocuSigned by:
BRENT LIN
38FA9C8D5943431...

BRENT LIN

Committee Members

Acknowledgments

This study would not have been possible without the guidance of my thesis committee mentors: Dr. Thomas Tanbonliong, Dr. Thuan Le, Dr. Brent Lin, and Dr. Sunita P. Ho.

Author Contributions

Conceptualization: Conrad Chou, Sunita P. Ho

Investigation: Conrad Chou, Misun Kang, Rosalyn Sulyanto, Dilworth Y. Parkinson, Sunita P. Ho

Methodology: Conrad Chou, Misun Kang, Rosalyn Sulyanto, Dilworth Y. Parkinson, Thuan Le, Sunita P. Ho

Data curation: Conrad Chou, Misun Kang, Rosalyn Sulyanto, Dilworth Y. Parkinson, Sunita P. Ho

Formal analysis: Conrad Chou, Rosalyn Sulyanto, Dilworth Y. Parkinson, Sunita P. Ho

Writing – original draft: Conrad Chou

Writing – reviewing and editing: Conrad Chou, Thomas Tanbonliong, Thuan Le, Brent Lin, Dilworth Y. Parkinson, Rosalyn Sulyanto, Sunita P. Ho

ABSTRACT

Silver Diamine Fluoride Differentially Affects Dentin and Hypomineralized Enamel Permeabilities

by Conrad Chou

INTRODUCTION: Permeabilities of enamel and dentin have implications on the symptoms and disease status of a patient with dentin caries and/or enamel hypomineralization. The purpose of the study is to investigate the effect of silver diamine fluoride (SDF) on physiochemical properties by correlating permeability with mineral density (MD) and elemental composition of hypomineralized enamel and carious dentin.

METHOD: Enamel and dentin from extracted carious primary teeth with (N=3;41 regions) and without (N=3;35 regions) SDF treatment *in-vivo*, and hypomineralized enamel from permanent molars with (N=4;10 regions) and without (N=7;41 regions) SDF treatment *in-vitro* were scanned using X-ray micro computed tomography. Spatial elemental maps of Zn^{2+} and Ca^{2+} were generated using X-ray fluorescence microprobe. Physicochemical properties were computed using Porous Microstructure Analysis, BoneJ, and RStudio software. Physicochemical effectors of tissue permeabilities were delineated using principal component analysis/regression.

RESULTS: Three dentin zones (carious; transparent; sound) of varying MD, diameter, and tubule occlusions were observed in carious primary teeth. Hypomineralized enamel exhibited variable severity and spacing between enamel rods. The intrinsic permeability of SDF-treated carious dentin (1.48e-14 +/- 7.11e-15 $1/m^2$), but not SDF-treated transparent dentin (1.82e-15 +/- 1.46e-15 m^2), was significantly lower than those of untreated carious dentin (1.48e-14 +/-7.11e-15 m^2; $P<0.0001$) and transparent dentin (1.61e-15 +/-9.44e-16 m^2; $P=0.9293$), respectively. Permeability of severely hypomineralized enamel (5.71e-15 +/- 2.04e-15 m^2) was comparable to adjacent sound dentin (5.28e-15 +/- 1.30e-15 m^2; $P=0.1409$), and was significantly higher than mildly hypomineralized enamel (1.39e-15 +/- 1.04e-15 m^2; $P<0.0001$). Surprisingly, the permeability of SDF-treated severely hypomineralized enamel (5.00-15 +/- 2.04e-15 m^2; $P=0.0693$) is not significantly different from that of untreated severely hypomineralized enamel. Principal component regression identified Zn^{2+} level ($P<0.0001$) and tissue anisotropy ($P<0.0001$) as significant effectors of tissue permeabilities. Principal component analysis and pairwise permutational multivariate analysis indicated that carious dentin with and without SDF and hypomineralized enamel are physiochemically distinct ($P<0.0001$).

CONCLUSION: Progression of caries is spatially and chemically dynamic. The physicochemical properties of SDF-treated carious dentin are likened to transparent dentin. Zn^{2+} localization can alter dentin and enamel permeability. Permeability of severely hypomineralized enamel is comparable to sound dentin. Permeability of non-carious hypomineralized enamel is unaffected by SDF treatment.

TABLE OF CONTENTS

LIST OF FIGURES

LIST OF TABLES

INTRODUCTION:

Permeabilities of enamel and dentin have implications on the symptoms and disease status of a patient with dentin caries and/or enamel hypomineralization. The hydrodynamic theory of dentin sensitivity states that a stimulus applied to exposed dentinal tubules causes movement of tubular fluid which stimulates nerve receptors. Any decrease in the functional radius of the dentinal tubules should greatly reduce the rate of fluid flow, thus reducing dentinal hypersensitivity.[1–3] Dentin permeability is an important factor determining pulp reactions to caries, operative procedures and other localized lesions affecting it.

Dental caries is a biofilm-mediated, sugar-driven, multifactorial, dynamic disease that results in the phasic demineralization and remineralization of dental hard tissues.[4] Dental caries remains the most prevalent chronic disease in both children and adults.[5] Structurally, carious enamel exhibit enlarged prism sheaths with diffuse mineral destruction in the prism cores.[6] In contrast, carious dentin manifests in the progression of sclerosis of the lumens of the dentinal tubules, gradient of demineralization of intertubular dentin, and destruction of occluded tubular lumens and peritubular dentin.[6] If the dentin is impermeable, either because of intratubular mineralization or due to a lack of tubular communication with reactive or reparative dentin, it will be able to prevent pulp damage even if toxic substances from caries or restorative materials are present.[1,2,7] It’s been well documented that the permeability of dentin decreases with age and carious lesion.[8,9] After excavation and removal of smear layer, carious dentin still exhibited markedly reduced permeability.[8]

Molar-incisor hypomineralization (MIH) is developmental defect caused by disruptions to the calcification or maturation processes of enamel.[10] The prevalence of MIH is estimated to be 14.2% globally. It is characterized by opacities ranging from creamy to brown and is chronologically and spatially variable even within the same individual.[11] MIH-affected enamel has a normal thickness of enamel but increased carbon content which reflects an increase in both carbonate and protein content.[12,13] Children with molar-incisor hypomineralization present several clinical problems, including rapid post-eruptive enamel breakdown, increased caries risk, dentin hypersensitivity, and aesthetic concerns.[11,12] Specifically, the severity of hypersensitivity varies but is frequently associated with the severity of hypomineralization and enamel loss.[14] Hypomineralized enamel shows thicker sheath structures surrounding the prisms, contributing to reduced hardness and elastic modulus.[15] Furthermore, MIH lesions exhibit substantial areas of increased porosity.[13]

Silver diamine fluoride (SDF) was cleared by the U.S. Food and Drug Administration in 2014 for the treatment of dentinal hypersensitivity. Systematic reviews have shown that the use of SDF is more effective in controlling or arresting caries than other treatments or placebos.[16–20] Greenhill and Pashley demonstrated that silver nitrate reduces the hydraulic conductance of dentin.[3] SDF has been shown to occlude dentinal tubules, producing preferential fluorohydroxy-apatite and increasing mineral density (MD) and hardness.[17,21,22] Silver chloride, metallic silver, silver phosphate, calcium fluoride, and silver-doped hydroxyapatite are formed after application of SDF.[17,22,23] In patients with

MIH, SDF may play a role in managing dentin hypersensitivity and in managing symptomatic MIH affected teeth.[20,24] SDF has been shown to be a clinically effective and safe tooth desensitizer.[25] Recent studies have confirmed that both SDF and silver-modified atraumatic restorative treatment can lead to favorable short-term prevention against dental caries while providing effective desensitization.[24,26] However, to the best of our knowledge, there is limited to no study that demonstrates the effects of SDF on the permeability of carious dentin or hypomineralized enamel.

Permeability of enamel and dentin has traditionally been measured based on passive diffusion of dye,[27,28] formation of micro-droplets,[29,30] fluid filtration under hydrostatic pressure,[3,8,9,31–33] or indirect imaging methods.[13,34,35] Given that interstitial fluid pressure in the pulp drives the fluid flow in dentin tubules, hydrostatic pressure is a crucial component in permeability measurement.[1,33] However, the aforementioned methods are met with limitations including, large minimum sample dimensions, influence of smear layer, storage condition, organic constituents, and difficulty in the standardization of permeability measurements. These limitations pose challenges to studying the permeability of human dental samples under different pathologic and treatment conditions.

It has been reported that the direction and density of dentinal tubules can be measured by X-ray tensor tomography.[36] While knowledge of the radius, length, and density of dentin tubules would allow theoretical calculation of hydraulic conductance through dentin tubules,[1,2] we postulated that micro-scale volumetric information of the dental

structure would allow precise simulation of fluid flow through the regions of interest. Here, we proposed the use of micro computerized tomography (microCT) to obtain 3D micro-architectures of carious dentin and hypomineralized enamel, through which computed physical properties including permeability could be spatially correlated with chemical characteristics. Specifically, we applied the present methodology to analyze the effect of silver diamine fluoride on carious dentin of primary teeth and molars diagnosed with MIH.

We hypothesized that changes in the micro-architecture of pathologic dentin and enamel manifest in shifts in MDs and can positively or negatively affect their permeabilities. The objectives of the study are: 1) to correlate the permeability of a) carious dentin and b) hypomineralized enamel with changes in respective physicochemical properties, and 2) to investigate the effect of SDF on carious dentin and hypomineralized enamel.

MATERIALS AND METHODS:

Specimen Collection:

Enamel and dentin were processed from extracted carious primary teeth with (N=3) and without (N=3) SDF treatment *in-vivo*, and hypomineralized permanent molars with (Severely hypomineralized, N=4) and without (Severe hypomineralized, N=3; mildly hypomineralized, N=4) SDF treatment *in-vitro*. Specimens were obtained from 3 to 10-year-old patients following an Institutional Review Board–approved protocol (IRB-P00025055) with MOU to UCSF – Ho Lab. Inclusion criteria for primary teeth were as

follows: American Society of Anesthesiology (ASA) I or II, primary teeth exhibiting caries that were directly accessible without removal of tooth structure with a dental handpiece. Inclusion criteria for permanent molars were as follows: ASA I or II, molars exhibiting enamel hypomineralization, and treatment planned for molar substitution. Exclusion criteria were patients with signs and symptoms of irreversible pulpitis or pulpal necrosis. For carious primary teeth, SDF (Advantage Arrest) was applied for 60s per the guidelines from the American Academy of Pediatric Dentistry.[37] Two SDF-treated teeth were treated 3 weeks prior to planned extraction; one was extracted 2 minutes after SDF treatment. For hypomineralized permanent molars, SDF was applied for 60s after extraction. Teeth were fixed in 10% neutral formalin solution and processed for laboratory analysis. See **Table 1** for summary of specimens used in the present study.

Table 1: Summary of pathologic dentin and enamel conditions, number of specimens, regions, and subvolumes selected for analysis.

	Carious Dentin No SDF	**Transparent Dentin No SDF**	**Sound Dentin No SDF**	**Carious Dentin SDF**	**Transparent Dentin SDF**	**Sound Dentin SDF**	**Hypomineralized Enamel Mild**	**Sound Dentin Hypomin Mild**	**Hypomineralized Enamel Severe**	**Sound Dentin Hypomin Severe**	**Hypomineralized Enamel Severe**
# Sample Teeth	3			3			4		3		4
# Regions	17	9	9	18	11	12	14	5	13	9	10
# Sub Volumes	104	34	55	68	53	82	84	40	92	72	80

X-ray Computed Tomography:

Extracted teeth were washed using 1x phosphate-buffered saline, dehydrated with 50-70% ethanol, and stored in 70% ethanol at 4C per establish protocol.[38] Specimens were cut into beams using low-speed water-cooled diamond saw (Isomet, Buehler, Lake Bluff, IL) (**Figure 1A.1 & 1B1**). Beams of 0.6 to 1 mm in length and width containing carious dentin or hypomineralized enamel were dried in room temperature and pressure. X-ray micro computed tomographies were obtained at beamline 8.3.2 of Advanced Light Source at Lawrence Berkeley National Laboratory. Specimens were imaged (pixel size: 0.65μm) at 20 or 25 keV of energy.

Mineral Density and Image Segmentation:

The reconstructed microCT 3D images of the specimens were analyzed with Avizo 2022.2 software (Fisher Scientific). Volumes containing carious dentin or hypomineralized enamel were segmented based on X-ray intensity and grayscale values of respective normal tissues within the specimens. For carious dentin of primary teeth, the segmentation threshold was set to 9-10% of the greyscale value of sound dentin; hypomineralized enamel of permanent teeth, 51-60% of the greyscale value of normal enamel; dentin of permanent teeth, 46-48% of the of the greyscale value of the underlying sound dentin. Mineral densities were calibrated by converting the observed greyscale values of sound dentin or enamel to reference mineral density values. The reference mineral density values (mg/cc) in primary teeth were obtained from calibrated measurements published in our previous study.[39] The reference mineral density values (mg/cc) in permanent teeth were based on Ho et al.[40] Observed differences in the greyscale values of pathologic tissues are proportional to changes in mineral densities.

Region of Interest Selection:

Selection for a region of interest to be used for analysis in carious primary teeth was based on the structural features of dentinal tubules in the segmented microCT 3D image (**Figure 1A.1,3 & 1B.2,3**). The following inclusion criteria applied: visible tubular structure within region of interest, location consistent with progression of caries (in the following order from surface of carious lesion: carious dentin, transparent dentin, and sound dentin), dentinal tubules without occlusion for sound dentin, dentinal tubules with evident occlusions for transparent dentin, and dentinal tubules with enlarged diameter or spacing for carious dentin. Additionally, regions of interest involving SDF-treated specimens, visible silver particles (as indicated by the presence of radiopaque speckles) must be present in carious dentin. Exclusion criteria were as the following: physical defects or cracks, lack of visible tubular structure, imaging artifacts including ring and truncation artifacts, region distant from carious lesion, presence of anatomic anomaly, and tissue with excessively low or high MD compared to reference normal dentin. Selection for a region of interest in molars with hypomineralization was based on structural features of the enamel rod sheaths and associated spacing in the segmented microCT 3D image. Inclusion criteria were as the following: presence of tubular to horseshoe-shaped spacing along the enamel rod, MD >15% loss compared to reference normal enamel for severe hypomineralization, MD <15% loss compared to reference normal enamel for mild hypomineralization. Exclusion criteria included: presence of caries, tissue with excessively low or high MD including severely de-

mineralized enamel or normal enamel without hypomineralization, physical defects or cracks, and the aforementioned imaging artifacts.

Elemental Mapping and Surface Morphology with X-ray Fluorescence Microprobe and FESEM:

Whole specimens were sectioned along a mesial-distal plane through the carious lesion with a slow speed saw. Elemental maps, including phosphorus (P^{3-}), calcium (Ca^{2+}), zinc (Zn^{2+}), and silver (Ag^{+}), were collected with an X-ray fluorescence microprobe (μXRF) at beamline 10.3.2 of Advanced Light Source at Lawrence Berkeley National Laboratory and SLAC National Accelerator Laboratory. Elemental distribution maps were collected with an incident beam energy of 10 keV and a spot size of ~20×20 μm. Following μXRF, the sectioned specimens were imaged with FESEM (field emission scanning electron microscopy; SIGMA VP500 Carl Zeiss Microscopy) at various magnifications at 1 keV to obtain secondary electron (SE) images.

Computational Physical Properties:

Physical properties were computed using Porous Microstructure Analysis (PuMA) version 3.0, ImageJ 1.53t, and BoneJ 7.0.14.[41–43] Regions of interest from the segmented microCT 3D image were processed into nonoverlapping 65x65x65μm subvolumes. Physical properties, including intrinsic permeability (unit = m^2), volume fraction (volume of solid / total volume), specific area (surface area / total volume, unit = 1/m), degree of anisotropy (0 to 1), mean thickness (unit = μm), and mean spacing (unit = μm), were computed for each subvolume. Permeability was based on the permeability

homogenization function using a Finite Element method, which approximates both the velocity and pressure fields with first-order elements.[44] Degree of anisotropy is a measure of how highly oriented substructures are within a volume, where zero indicates no orientation within a volume, and was obtained using the mean intercept length.[45] Thickness or spacing at a point was defined as the diameter of the greatest sphere that fitted within the structure or space and which contained the point.[46] Velocity field data from permeability computation was rendered using ParaView 5.10.1.[47]

Correlative Image Analyses of Physical Properties, MD, and Elemental Maps:

For spatial correlation of elemental (P^{3-}, Ca^{2+}, Zn^{2+}, Ag) maps, 5 to 20 X-ray tomograms (number of tomograms depended on specimen size) were selected and averaged to account for the μXRF penetration depth.[39] Elemental maps were analyzed with ImageJ 1.53t for colocalization of elements and subsequent correlation of colocalized elements with physical properties and MD. In carious primary teeth, two-dimensional correlative plots of elements from the surface of carious lesion to sound dentin were generated. The junction between transparent dentin and sound dentin was used as the reference for spatial correlation of physical properties, MD, and elemental maps.

Statistics:

Descriptive statistics, Mann Whitney test, Kruskal–Wallis one-way analysis of variance, and multiple linear regression were completed using GraphPad Prism 9.4.1.[48] Principal component analysis / regression, nonnegative matrix factorization, Kolmogorov-Smirnov test, and permutational multivariate analysis of variance were performed using RStudio

1.53t and related software packages.[49–54] Frequency histograms, ridgeline plots, violin plots, and scatter plots were generated using GraphPad Prism 9.4.1 and RStudio 1.53t.[48–51,55,56]

RESULTS:

Micro-Architecture and Fluid Flow Simulation:

SDF-treated carious dentin displayed pronounced staining indicating effectiveness of treatment *in-vivo* (**Figure 1A.1,2**). Tomographs from microCT revealed three dentin zones in carious primary teeth: carious, transparent, and sound dentin of varying mineral density, diameter, tubule occlusions, and silver particles (**Figure 1A.3**). Hypomineralized enamel exhibited characteristic yellow to brown demarcated enamel opacities (**Figure 1B.2**). Remarkably, tomographs from microCT showed widened enamel sheaths and variable spacing between the rods (**Figure 1B.3**).

SEM and microCT images illustrated the changes in micro-architecture of pathologic dentin and enamel (**Figure 2A1,2-F1,2**). Segmented microCT 3D data and rendered representative volumes (65x65x65µm) of tissue types further demonstrated these architectural changes. Location-specific flow velocity vectors along the dentin tubules or enamel rods represent altered fluid flow affected by caries or hypomineralization (**Figure 2A4-F4**). Specifically, sound dentin exhibited a high number of above-average flow velocity vectors, high degree of tubules orientation (high degree of anisotropy), and uniform fluid flow. On the other hand, untreated carious dentin showed drastically increased number of high flow velocity vectors, non-uniform fluid flow, and increased

spacing secondary to structure loss (reduced volume fraction). However, transparent dentin demonstrated obstructed, non-uniform fluid flow, and markedly reduced spacing. Notably, SDF-treated carious dentin showed increased tubule occlusion and reduced fluid flow compared to carious dentin without SDF, though the fluid flow remained non-uniform. Severely hypomineralized enamel exhibited gapping between enamel rods forming spaces to allow fluid flow. In contrast, mild hypomineralized enamel displayed reduced spacing between enamel rods, leading to reduced number and magnitude of flow velocity vectors. Some volumes of hypomineralized enamel were affected by caries as indicated by reduced MD, hence, not selected for computation.

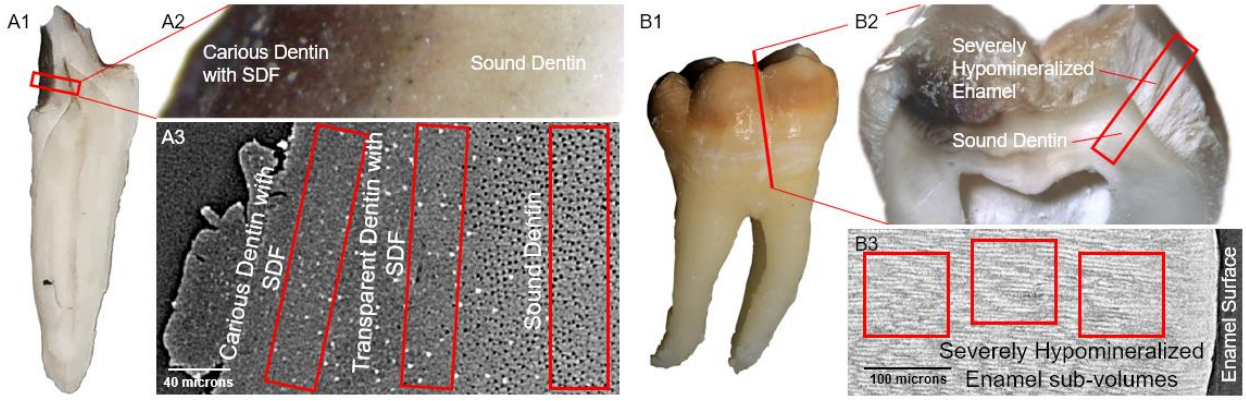

Figure 1: Sample processing and microCT visualization. **A1,B1**: Photos of a carious primary tooth treated with SDF *in-vivo*, and permanent molar with severe hypomineralization without SDF. **A2,B2**: Light microscope image of specimens showing changes in the color and texture of tissues. **A3,B3**: Tomographs from microCT revealing three dentin zones: carious, transparent, and sound dentin of varying mineral density, diameter, tubule occlusions, and silver particles. Hypomineralized enamel showed widened enamel sheaths and gapping between the rods.

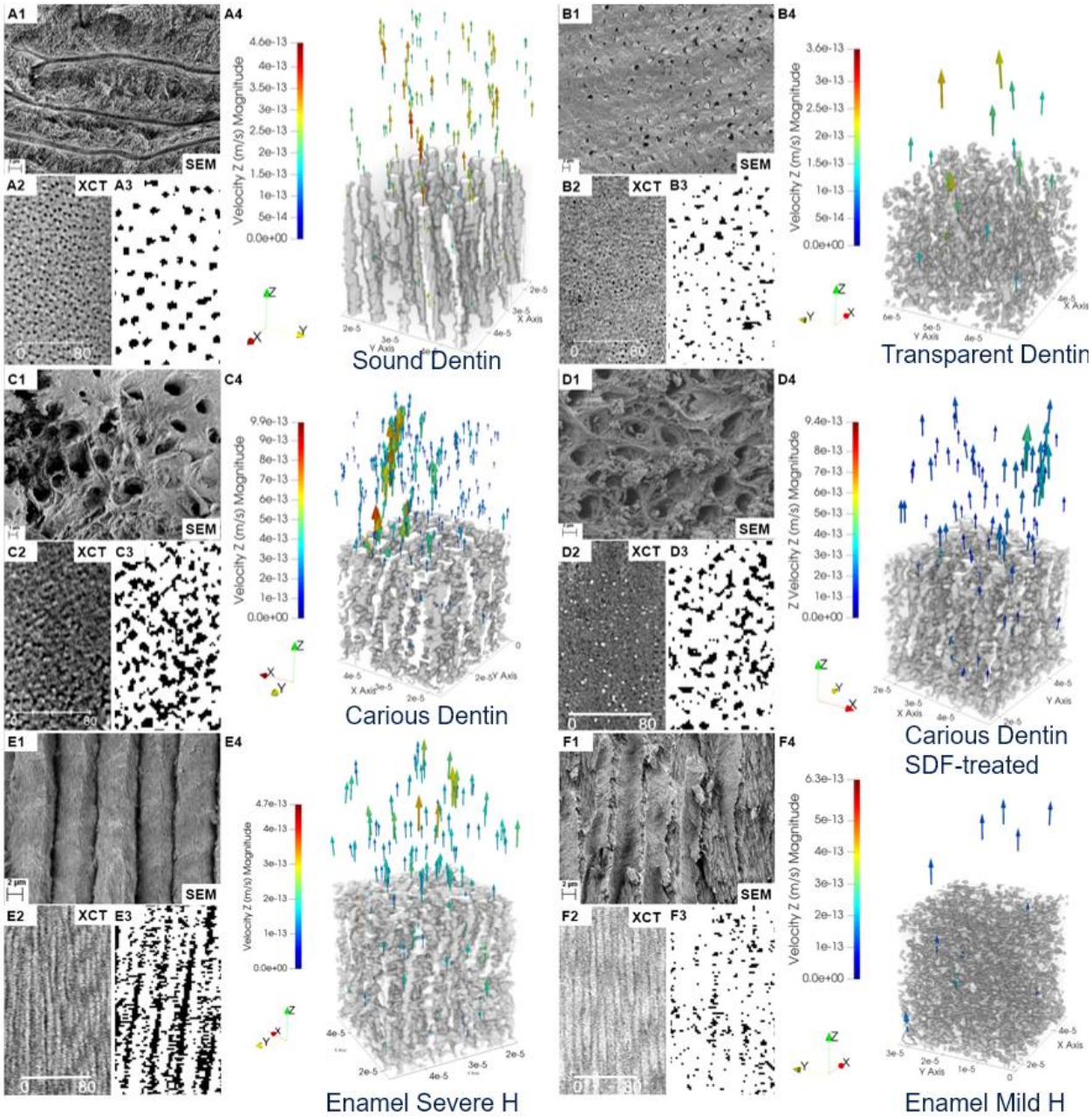

Figure 2: Flow simulation and micro-architecture. Changes in micro-architecture of pathologic dentin and enamel manifested in altered fluid flow. **A1-C1**: Scanning electron microscope (SEM) images showing the dynamic changes in the dentin tubules as a result of sclerosis, and carious progression. **A2-C2**: microCT image slices showing tubule occlusions and destructions. **A4-C4**: Simulated fluid flow through representative subvolumes of sound dentin, transparent dentin, and carious dentin, respectively. Vector arrows indicate magnitude (m/s) and location of fluid flow in Z-direction, along dentin tubules. White structure denotes tubule spaces. **D1-D3**: SEM, microCT, and flow simulation in SDF-treated carious dentin. **E1-3, F1-3**: SEM, microCT, and flow simulation in enamel with severe and mild hypomineralization, respectively.

Flow Profiles:

The flow velocity vectors of representative volume for each tissue type were summarized in frequency histograms (**Figure 3**). Two-sample Kolmogorov-Smirnov tests indicated that frequency histogram of the flow velocities of SDF-treated carious dentin, untreated carious dentin, transparent dentin have distinct distributions ($P<0.005$ for all pair-wise tests). Likewise, significantly different flow velocities distributions were demonstrated in severely hypomineralized enamel, mildly hypomineralized enamel, and sound dentin ($P<0.005$ for all pair-wise tests). However, sound dentin adjacent to severely or mildly hypomineralized enamel showed similar flow velocities distributions ($P>0.05$).

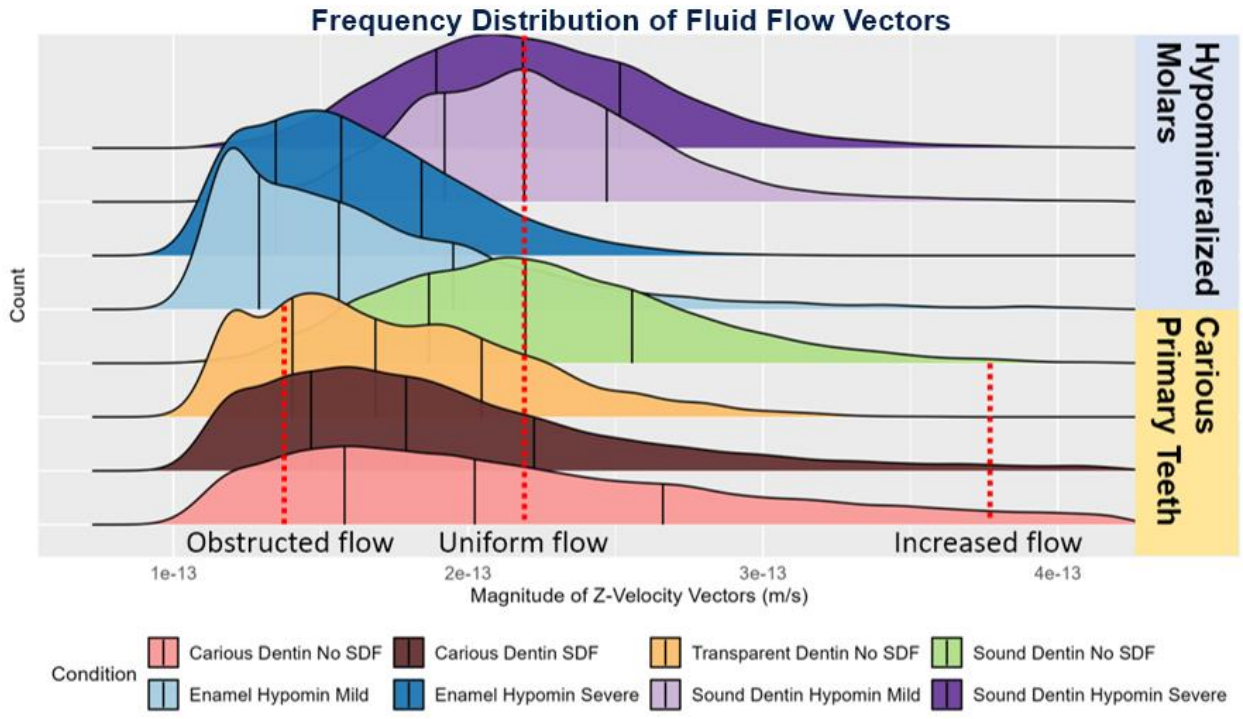

Figure 3: Flow profiles of dental tissues in health and disease. Carious dentin, transparent dentin, and hypomineralized enamel (mild or severe) showed skewed, non-uniform flow. Sound dentin displays symmetric and uniform flow. Heavy right-sided tail

in carious dentin drove fluid flow. SDF-treated carious dentin demonstrated a flow profile characteristic between untreated carious and transparent dentin.

The flow velocities of sound dentin, in both carious primary teeth and molars with enamel hypomineralization, demonstrated symmetry and strong central tendency, whereas in all pathologic dentin and enamel, the flow velocities exhibited asymmetry with varying degrees of right-sided skewness. Notably, the magnitude of flow velocities of SDF-treated carious dentin (2.04e-13 +/- 9.01e-14 m/s) lie between those of untreated carious (2.49e-13 +/- 1.24e-13 m/s) and transparent dentin (1.75-13 +/- 4.47e-14 m/s). However, the number of non-zero flow velocity vectors between SDF-treated carious dentin (N=27359) and untreated carious dentin (N=27570) are not significantly different, while it is drastically reduced in transparent dentin (N=3847). The shift to toward low number and low magnitude of velocity vectors indicated increased obstruction of tubular spaces. The heavy right-sided tail of flow velocities in untreated carious dentin, which contributed the high permeability of carious dentin, was markedly reduced after SDF treatment.

The mean flow velocities of severely hypomineralized enamel (9.2e-14 +/- 1.35e-13 m/s) was lower and more varied than those of sound dentin (2.22e-13 +/- 4.67e-14 m/s). However, the number of non-zero velocity vectors was drastically higher in severely hypomineralized enamel (N=41017) than the adjacent sound dentin (N=22897), equivocating the intrinsic permeability of severely hypomineralized enamel as compared to the adjacent sound dentin. Contrariwise, mildly hypomineralized enamel showed

increased mean flow velocity (9.59e-14 +/- 1.29e-13 m/s) but heavily reduced number of velocity vectors (N=5866) versus severely hypomineralized enamel.

MDs and Computed Physical Properties:

MDs and computed physical properties, including intrinsic permeability (m^2), volume fraction (0-1), degree of anisotropy (0-1), mean thickness (µm), and mean spacing (µm), of dentin and enamel tissues were summarized in **Figure 4**. Kruskal–Wallis one-way analysis of variance tests confirmed differences among the tissue types for MD and each of computed physical properties ($P<0.0001$). The distributions of MDs and computed physical properties overall varied from bell-shaped to bimodal, and exhibited wide spread and skewness. Pair-wise Mann Whitney tests were used for statistical comparisions of MDs and physical properties between tissue types.

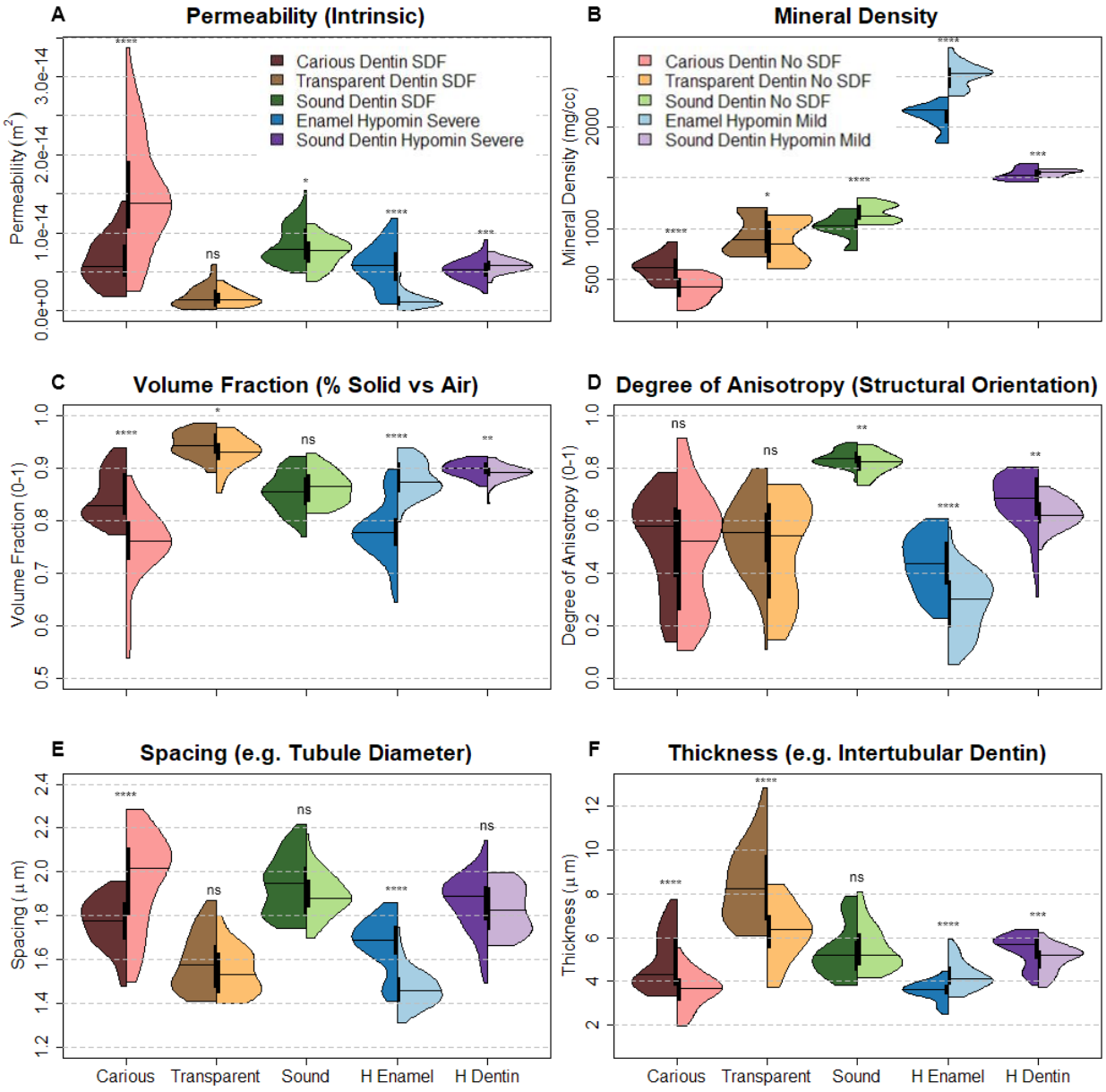

Figure 4: MD and computed permeability and associated physical properties. Statistical significances are provided for tissue types juxtaposed on violin plots (SDF-treated versus untreated tissue; severely versus mildly hypomineralized enamel). ns=not significant; *P<0.5; **P<0.01; ***P<0.001; P****P<0.0001.

The MD of SDF-treated carious dentin (612.6 +/-124.6 mg/cc) was higher than untreated carious dentin (407.1 +/-119.0 mg/cc; P<0.0001). SDF-treated transparent dentin (940.8 +/-186.0 mg/cc) also showed higher MD than untreated transparent dentin

(885.4 +/-215.2 mg/cc), although this observed difference approached non-significance (P=0.0497). The MDs of carious and transparent dentin overall were markedly lower than those of treated or untreated sound dentin, which ranged from 780.9 to 1298 mg/cc. The MD of severely hypomineralized enamel (2103 mg/cc +/- 126.1 mg/cc) was on average 24.6% lower than reference normal enamel,[40] and was significantly lower than that of mildly hypomineralized enamel (2514 +/- 118.9 mg/cc; P<0.0001). The MDs of sound dentin adjacent to severely and mildly hypomineralized enamel were 1536 +/- 58.02 and 1552 +/-30.71 mg/cc, respectively.

The intrinsic permeability of SDF-treated carious dentin (1.48e-014 +/- 7.11e-15 m^2), but not SDF-treated transparent dentin (1.82e-15 +/- 1.46e-15 m^2), was significantly lower than those of untreated carious dentin (1.48e-14 +/-7.11e-15 m^2; P<0.0001) and transparent dentin (1.61e-15 +/-9.44e-16 m^2; P=0.9293), respectively. Permeability of severely hypomineralized enamel (5.71e-15 +/- 2.04e-15 m^2) was comparable to the adjacent sound dentin (5.28e-15 +/- 1.30e-15 m^2; P=0.1409), and was significantly higher than mildly hypomineralized enamel (1.39e-15 +/- 1.04e-15 m^2; P<0.0001). Surprisingly, the permeability of SDF-treated severely hypomineralized enamel (5.00e-15 +/- 2.04e-15 m^2; P=0.0693) was not significantly different from that of untreated severely hypomineralized enamel, indicating that SDF treatment *in-vitro* did not alter the permeability of hypomineralized enamel.

Figure 5 delineated the relationships between permeability and associated MD and physical properties, including specific area (1/m). In carious primary teeth, multiple

linear regression showed that MD and all computed physical properties, except degree of anisotropy (P=0.1078), were significant effectors of permeability (P<0.001). Volume fraction and specific area most significantly correlated with permeability, while thickness and spacing served as least significant covariates. In permanent molars with enamel hypomineralization, all physical variables were significant effectors of permeability, with volume fraction and specific area also showing highest levels of significance. Interestingly, MD was observed to be a weak but significant effector of permeability in both carious primary teeth and permanent molars with enamel hypomineralization (P<0.0001). Strong multicollinearity existed among all computed physical properties with R2 ranging from 0.7419 to 0.9824. The residual plots of both carious primary teeth and permanent molars with enamel hypomineralization revealed non-random pattern, suggesting a non-linear relationship between permeability and covariates.

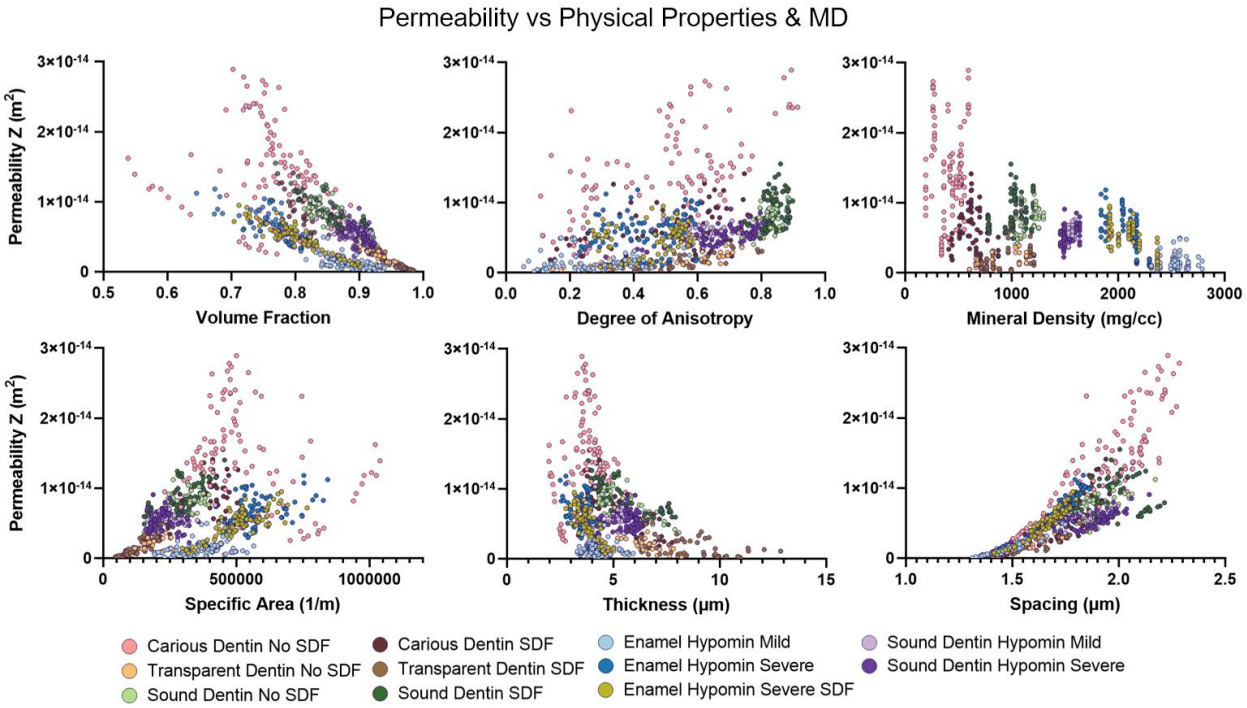

Figure 5: Permeability versus MD and physical properties. The permeabilities of dentin and enamel were non-linearly correlated with their physical and chemical properties. Strong multicollinearity existed among all variables.

Principal Component Analysis:

Principal component analysis (PCA) and pairwise permutational multivariate analysis of MD and computed physical properties indicated that the centroids of all tissue types in primary carious teeth, except SDF-treated versus untreated sound dentin, were physically distinct ($P<0.001$). The first two principal components explained 89.31% of variance and defined the observed centroids. The Euclidean distances among the centroids of tissue types demonstrated that SDF-treated transparent dentin and untreated carious dentin were most physically distinct (distance = 4.790; adjusted $P<0.05$), whereas SDF-treated versus untreated sound dentin were not physically distinct (distance = 0.1561; adjusted $P=0.900$). Importantly, the centroids between SDF-treated and untreated carious dentin were significant different (distance = 2.023; adjusted $P<0.05$), confirming that SDF treatment not only reduced the permeability of carious dentin, but also altered the overall physical properties of the material. Furthermore, the centroid of SDF-treated carious dentin shifted toward those of SDF-treated and untreated transparent dentin, indicating that the physical properties of SDF-treated carious were likened to those of transparent dentin.

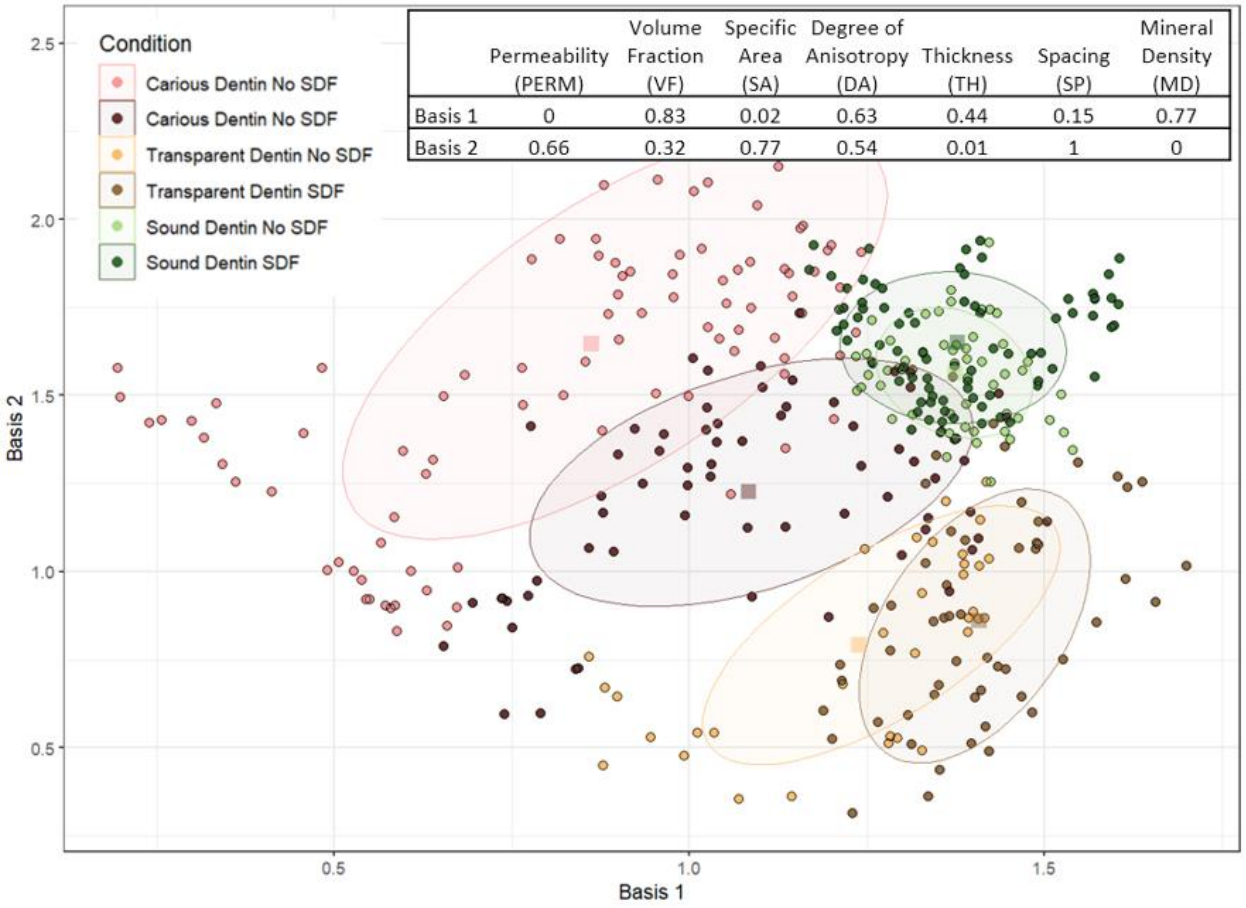

	Permeability (PERM)	Volume Fraction (VF)	Specific Area (SA)	Degree of Anisotropy (DA)	Thickness (TH)	Spacing (SP)	Mineral Density (MD)
Basis 1	0	0.83	0.02	0.63	0.44	0.15	0.77
Basis 2	0.66	0.32	0.77	0.54	0.01	1	0

Figure 6: Cluster analysis of physical properties in SDF-treated and untreated carious primary teeth. All seven studied variables were summarized via non-negative matrix factorization into basis 1 and basis 2. The loadings of basis 1 and basis 2 are provided. Colored squares denote the centroids of respective tissue types. Each confidence ellipse captures data points within one-standard deviation from respective centroid. The centroid of SDF-treated carious dentin lied between those of untreated carious dentin and transparent dentin (both SDF-treated and untreated).

In permanent molars with enamel hypomineralization, PCA demonstrated that the centroids of SDF-treated and untreated severely hypomineralized enamel were not significantly different (distance = 0.4881; adjusted P=0.26), indicating that SDF treatment *in-vitro* did not alter the physical properties of severely hypomineralized enamel. Furthermore, the centroids of severely hypomineralized enamel were significantly different from that of mildly hypomineralized enamel (SDF-treated: distance

= 2.754; adjusted P<0.01; untreated: distance = 3.077; adjusted P<0.01). Furthermore, the centroids of SDF-treated and untreated severely hypomineralized enamel lied between those of sound dentin and mildly hypomineralized enamel, indicating that severely hypomineralized enamel exhibited more sound dentin-like physical properties compared to mildly hypomineralized enamel. The centroids of sound dentin adjacent to mildly versus severely hypomineralized enamel appeared apart, with their difference approaching significance. The first two principal components explained 93.78% of variance.

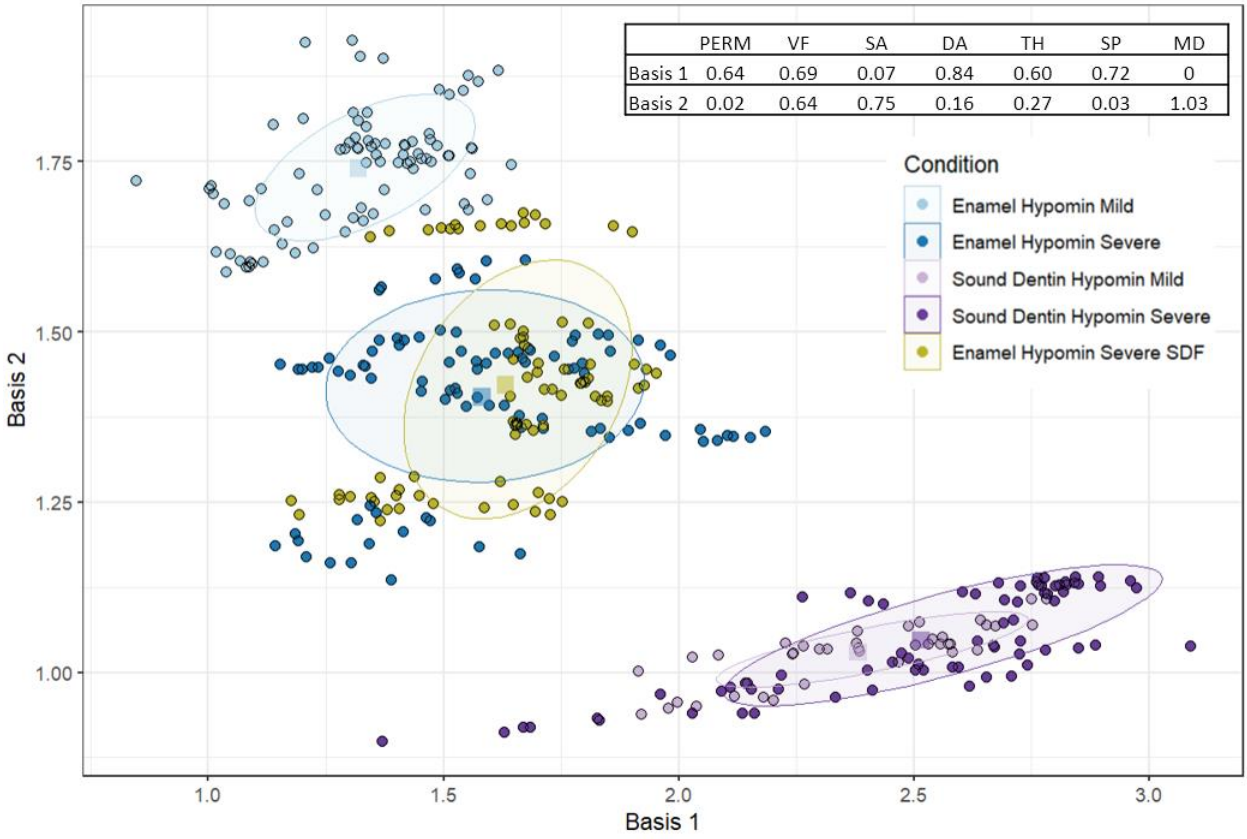

Figure 7: Cluster analysis of physical properties in permanent molars with hypomineralized enamel. The loadings of basis 1 and basis 2 are provided. Colored squares denote the centroids of respective tissue types. Each confidence ellipse captures data points within one-standard deviation from respective centroid. The centroids of SDF-treated and untreated severely hypomineralized enamel were not significantly different.

Elemental Composition Maps:

Figure 8 summarized the x-ray fluorescence microprobe elemental composition maps of carious dentin (SDF-treated and untreated) and severely hypomineralized enamel. In carious primary teeth, the levels of Ca^{2+}, P^{3-}, and Zn^{2+} across carious dentin, transparent dentin, and sound dentin were displayed from the surface of carious lesion to the sound dentin near the dental pulp at multiple regions. A steady increase in MD and Ca^{2+} levels corresponded to the reference locations beyond which physically sound dentin was observed. Aligning the levels of Ca^{2+}, P^{3-}, and Zn^{2+} based on the reference locations revealed that between carious and transparent dentin, Ca^{2+}, P^{3-}, and Zn^{2+} levels generally increased, whereas between transparent dentin and sound dentin, local minima of Ca^{2+} and P^{3-} levels were seen despite variations between the elemental maps (**Figure 8 A.4-5,B.3-4**). In the SDF-treated specimen, high levels of Ag^{+} were detected in carious dentin, beyond which the levels of Ag^{+} decreased steadily (**Figure 8 A.7**). However, the levels of Zn^{2+} in sound dentin remained high on the elemental map of SDF-treated specimen, but decreased drastically on that of untreated specimen (**Figure 8 A.6,B.5**). Additionally, the observed elemental composition patterns showed radial symmetry about the center of carious lesion. Location-specific Ca^{2+}, P^{3-}, and Zn^{2+} level scales were generated for SDF-treated and untreated carious primary teeth. In permanent molar with severely hypomineralized enamel, a heightened Zn^{2+} level was found throughout the pathologic enamel compared to the adjacent sound dentin. The overall uniformity of Ca^{2+}, P^{3-}, and Zn^{2+} levels reflected the observed uniform appearance of hypomineralized enamel and sound dentin as shown in **Figure 1 B.1**.

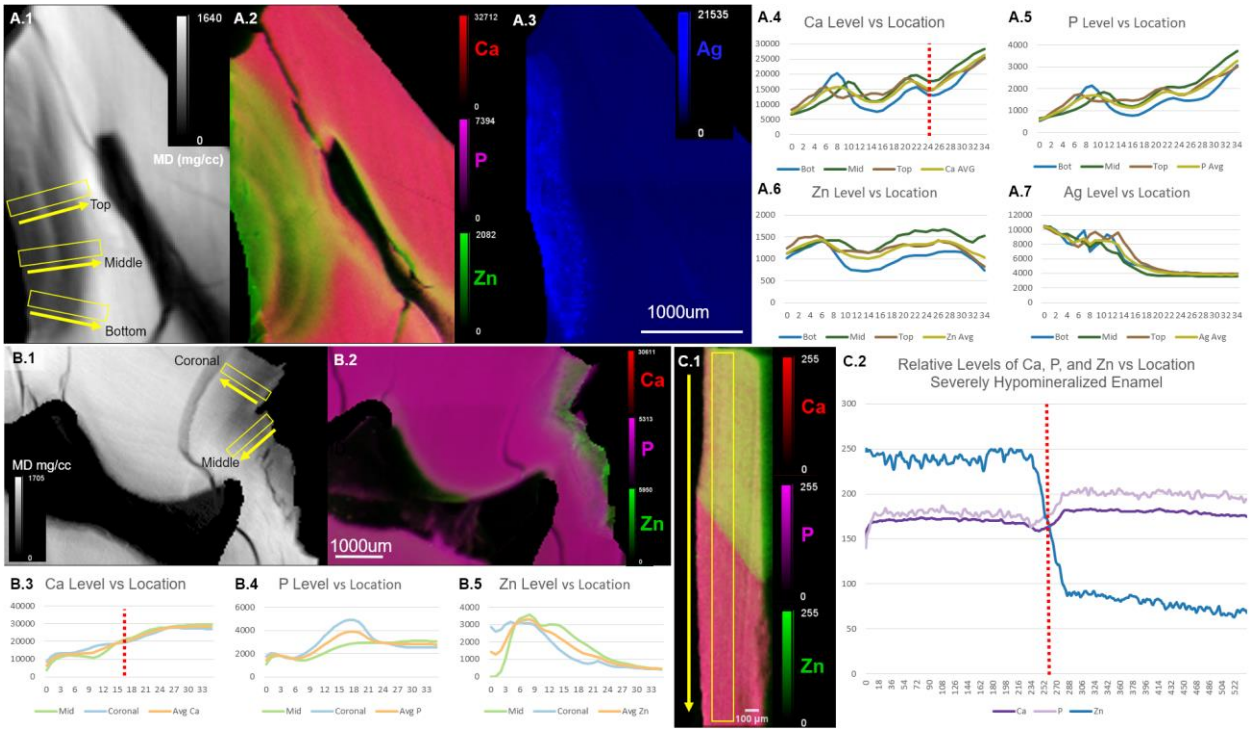

Figure 8: Elemental composition maps of primary carious dentin and severely hypomineralized enamel. **A.1,B.1**: Calibrated MD (white) maps generated from microCT of a SDF-treated and untreated carious primary tooth, respectively. **A.2-3**: corresponding x-ray fluorescence microprobe elemental maps of Ca^{2+} (red), P^{3-} (pink), and Zn^{2+} (green) in overlay, and Ag^{+} (blue) of the same SDF-treated specimen. **A.4-7**: levels of Ca^{2+}, P^{3-}, Zn^{2+}, and Ag^{+} versus distance from the surface of SDF-treated carious lesion at various regions, which are shown in yellow boxes **A.1. B.2**: elemental map of Ca^{2+}, P^{3-}, and Zn^{2+} in overlay corresponding to the untreated carious tooth of **B.1. B.3-5**: levels of Ca^{2+}, P^{3-}, and Zn^{2+} versus distance from the surface of untreated carious lesion at two regions, which are shown in yellow boxes in **B.1. C.1**: scalarized elemental map of Ca^{2+}, P^{3-}, and Zn^{2+} of the specimen with severely hypomineralized enamel shown in **Figure 1 B.1**. Top portion describes severely hypomineralized enamel; bottom portion, adjacent sound dentin. **C.2**: relative levels of Ca^{2+}, P^{3-}, and Zn^{2+} versus distance from the top surface of severely hypomineralized enamel. Red dotted lines in **A.4** and **B.3** represent the locations beyond which physically sound dentin was observed. Red dotted line in **C.2** denotes dentinoenamel junction. Yellow arrows specify the direction of location marks.

PCA of both physical and chemical properties, including Ca^{2+}, P^{3-}, and Zn^{2+} levels, revealed that all tissue types in primary carious teeth, including SDF-treated and untreated sound dentin, were physiochemically distinct ($P<0.001$). The first two principal components explained 73.06% of variance. Compared to the results of **Figure 6**, the

Euclidean distances among the centroids of SDF-treated carious dentin, transparent dentin, and sound dentin became further apart from their untreated counterpart when Ca^{2+}, P^{3-}, and Zn^{2+} levels were included in the PCA. Remarkably, SDF-treated carious dentin was further likened to transparent (both SDF-treated and untreated), while on the other hand, the distance between the centroids of SDF-treated and untreated sound dentin attained statistical significance (distance = 1.519; $P<0.05$). Principal component regression of physical and chemical properties indicated that all studied variables, including Zn^{2+} level, were significant effectors of tissue permeabilities ($P<0.0001$). Thickness, volume fraction, and specific area most significantly correlated with permeability, while MD, Ca^{2+} level, and degree of anisotropy served as least significant covariates.

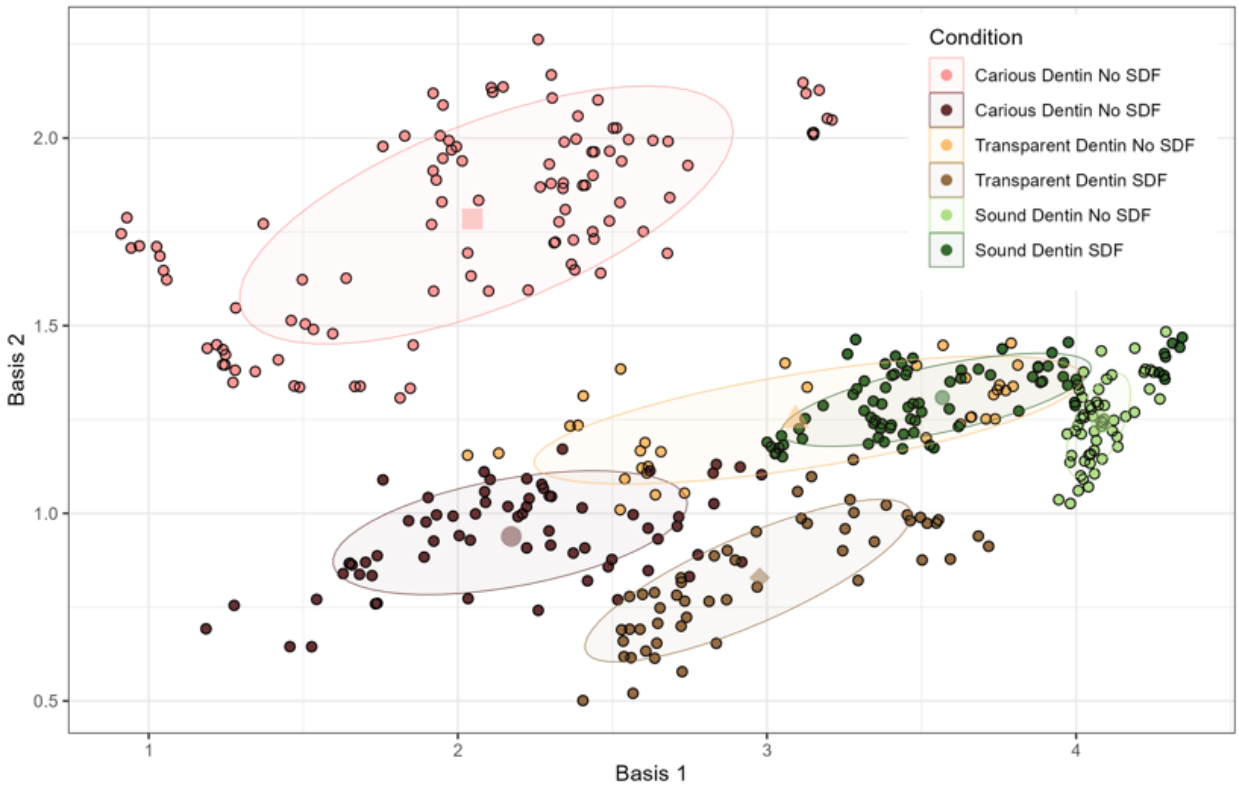

	PERM	VF	SA	DA	TH	SP	MD	Ca	P	Zn
Basis 1	0.09	1.09	0.11	0.99	0.57	0.46	1.05	0.63	0.59	0.09
Basis 2	0.40	0.29	0.50	0.27	0.03	0.53	0.00	0.05	0.17	0.79

Figure 9: Cluster analysis of physical and chemical properties in SDF-treated and untreated carious primary teeth. All ten studied variables were summarized via non-negative matrix factorization into basis 1 and basis 2. The loadings of basis 1 and basis 2 are provided. Colored squares denote the centroids of respective tissue types. Each confidence ellipse captures data points within one-standard deviation from respective centroid. Compared to **Figure 6**, the centroids of SDF-treated carious dentin, transparent dentin, and sound dentin became further distanced from their untreated counterpart when Ca^{2+}, P^{3-}, and Zn^{2+} levels were included in the PCA.

DISCUSSION:

Dentin Caries:

The microCT, SEM, and x-ray fluorescence microprobe data of the present study illustrated that the progression of caries is spatially and chemically dynamic. While the carious dentin signifies the progression of a chronic infectious disease, the transparent

dentin represents the pulp-mediated host response to pathogens. It is therefore of importance to corroborate our observed findings with known intricacies of dentin sclerosis. The odontoblast processes in carious dentin extend throughout the whole thickness of sound dentin and the inner carious dentin, accounting for the sense of pain and the ability for remineralization by transportation of ions.[57,58] Intratubular calcification, involving both hydroxyapatite crystals and whitlockite crystals, can occur by an initial mineralization of the peri-odontoblastic space followed by calcification of the odontoblast process.[58] It may also occur by an intracytoplasmic mineralization of the process, which serves as a matrix, followed by a secondary peri-odontoblastic mineralization.[6,59] If the odontoblasts have been irritated but not destroyed, they can increase their rate of secretion and mineralization of dentin matrix, lowering permeability.[2] The dynamically occluded dentinal tubules observed in both carious and transparent dentin of the present study were consistent with the above findings in cariology literature.

The dynamic nature of caries lesion progression urges that the classification of caries lesions makes distinctions in activity status.[60] In arrested caries, intertubular zone near surface is more mineralized with bacterial bodies coalescing in intratubular space. In the deeper layers, the intratubular contents were hypermineralized and appeared continuous with the peritubular zone [61] While there remains a need for standardization of caries activity assessment,[62] Nyvad et al. demonstrated that clinical diagnostic criteria including sound, inactive non-cavitated, active non-cavitated, and cavitated have predictive validity for the progression of caries lesion.[63,64] Recent cohort studies further

showed that caries progression rates are higher in caries-active individuals than those with inactive-caries clinical assessment, which based on the color and texture of enamel and dentin lesions.[65,66]

In the present study, our carious dentin samples, both SDF-treated or non-SDF-treated, were obtained from patients with severe early childhood caries. It is likely the case that all of our carious dentin samples contained active carious lesion, not arrested lesions. Our previous study showed that hypermineralized dentin in carious regions exhibited significantly higher MDs (1815-2740mg/cc) than sound dentin (1480-1590mg/cc).[40] However, in the present study, the MDs of transparent dentin, both SDF-treated and non-SDF-treated, were higher than carious dentin, but lower than sound dentin. This suggests that these transparent dentin regions represented those of active carious region with reduced permeabilities. A fully sclerosed dentin region in inactive caries may exhibit drastically higher MDs than sound dentin and impermeability. Additionally, the reduction in permeability due to the deposition of atubular reparative dentin may merit further investigation.

Given the potentials of the dentin-pulp complex to sclerose and create a nearly impermeable barrier against pathogens, restorative techniques resulting in complete coronal seal would implicate entombment of the pathogens within the tubule spaces. This helps explain the high survival rates of restorations using indirect pulp capping or the Hall technique, where caries were not excavated but isolated from the oral cavity by a crown or restorative material.[67,68] Conversely, complete excavation of caries not only

may disturb the enabling micro-environment of the dentin-pulp complex to sclerose dentin tubules and form tertiary dentin, but also subject the pulp to additional physicochemical insults. Linking altered permeability of dentin near pulp to measurable indicators of pulpal health, including levels of Zn^{2+} and other inflammatory markers, may further elucidate the biochemical mechanism of dentin sclerosis.

Enamel Hypomineralization:

In the present study, the microCT and SEM data of hypomineralized enamel supported existing literature. It has been shown the widened and de-mineralized enamel sheaths in carious enamel formed pathways of diffusion.[69] The predominantly organic enamel sheaths in normal enamel were reported to be 800–1000 nm in width.[70] Notably, the widened, porous, and proteinaceous enamel sheaths in hypomineralized enamel exhibited spacing between enamel rods.[13,71–75] Studies by Fagrell et al. demonstrated the presence of bacteria between the enamel rods and penetration of bacteria through intact hypomineralized enamel.[75,76] The variations in the spacing observed can be attributed to the variable nature of hypomineralization, including varying density of sheath regions, irregular distribution of prisms, and presence of interconnecting apatite crystals.[15,77]

Given that the MD of normal enamel vary between teeth within the same individual and that developmentally acquired enamel hypomineralization may differ from one region to another within a tooth, the assessment and categorization of enamel hypomineralization posed challenges. The MD of severely hypomineralized enamel has been shown to be

more than 15-20% lower than normal enamel.[12,13] In the present study, we used 15% reduction in MD as the cutoff to differentiate severe and mild enamel hypomineralization. However, broad ranges of MDs were observed with mild hypomineralization ranging from 4.73 to 14.24% and severe hypomineralization ranging from 15.1 to 34.6% de-mineralization. As shown in the PCA of **Figure 7**, enamel hypomineralization exhibited a dynamic continuum of MDs and physical properties when mildly and severely hypomineralized enamel were visualized as a whole. On this continuum of enamel hypomineralization, it remains daunting to decipher on where do clinical symptoms, including hypersensitivity and enamel breakdown, more frequently occur.

The present study supported that the permeability of severely hypomineralized enamel is comparable to sound dentin. We also demonstrated that sound unexposed dentin below hypomineralized enamel was morphologically unchanged, consistent with previous report.[78] Interestingly, Linner et al. showed that a significantly lower level of hypersensitivity is found for MIH patients older than 8 years of age and concluded that MIH related tooth hypersensitivity is most likely linked to the few years immediately after tooth eruption.[14] It remains unknown whether hypersensitivity associated with enamel hypomineralization is due to exposed dentin secondary to caries and/or enamel breakdown, or due to the permeable nature of severely hypomineralized enamel. The resolution of symptom in the former case would be suggestive of physiological dentine formation and reactive dentine apposition, while in the latter case, surface mineralization of hypomineralized enamel must have occurred prior to dentinal

adaptation to environmental insults. Further elucidation of the mechanisms to resolve MIIH-related hypersensitivity would be of tremendous clinical value.

Permeability Measurement:

It had been demonstrated that the measured hydraulic conductance generally is markedly lower than theoretical values because dentinal tubules contain debris and collagen fibers that contribute much more to the resistance of fluid movement than the microscopic dimensions of the tubules would predict.[32] In fact, organic constituents such as plasma, saliva and bacteria have been shown to cause pronounced reduction in dentin permeability.[31] While the present method of our study mainly accounted for inorganic constituents of the micro-architecture, the benefits of our method included the following: 1) measurement of volumetric intrinsic permeability that is unaffected by sample size or thickness, and presence of smear layer, surface mineralization, microcracks, or gross sample defects, 2) measured permeabilities that are correlated to other physical parameters, accounting for differences due to location of sample (coronal versus cervical), age of patient (increased tubule occlusion with age), and anatomical variations, 3) measurable variations in permeabilities and material properties across 65µm voxel sub-volumes, 4) measurement of permeability that is unaffected by radiolucent or predominantly organic constituents, and importantly 5) methodology that is non-destructive allowing subsequent correlational imaging and analysis.

It did not escape our notice that the permeabilities of SDF-treated (8.60e-15 +/- 2.39e-15 m^2) and untreated sound dentin (7.46e-15 +/-1.82e-15 m^2) were close but

significantly different (P=0.0260). However, the associated physical properties of SDF-treated and untreated sound dentin were consistent with and account for the difference in their permeabilities. Specifically, the mean diameters of the dentinal tubules (mean spacing) of SDF-treated sound dentin (1.938 +/- 0.131 μm) was measured to be higher than that of untreated sound dentin (1.892 +/- 0.0942 μm), though this difference was found to be insignificant (P=0.0660). Further, the thickness of dentin surrounding the dentinal tubules, that is, the sum of peritubular dentin and intertubular dentin, of SDF-treated (5.423 +/- 1.163 μm) was lower but insignificantly different from that of untreated sound dentin (5.479 +/- 0.969 μm; p=0.5327). Likewise, the volume fraction SDF-treated sound dentin (0.8557 +/-0.03752) was lower than that of untreated sound dentin (0.8638 +/-0.2988), but the difference was also not significant (P=0.2743). The measured significant difference in mean permeabilities of SDF-treated and untreated sound dentin appeared to be the cumulative effect of correlated physical properties. By accounting for differences due to location of sample, age of patient, and anatomical variations, we deemed the observed permeabilities valid for comparisons among healthy and pathological tissue types.

Effects of Silver Diamine Fluoride:

Our study illustrated that SDF-treated carious dentin has reduced permeability compared to untreated carious dentin, and that SDF-treated carious dentin is physiochemically likened to dentin undergoing sclerosis. Of importance, the SDF-treated carious sample teeth of the present study were exposed to the one-time effect of SDF from minutes to weeks, suggesting that the observed differences in the

permeability and mineral density could be attributed to the immediate effects of crystals and silver precipitates. In both cases, dense granular structures of spherical grains were found in the intertubular area of dentin after treatment with SDF, consistent with existing literature.[23] It should be noted that the mechanisms of SDF further include bactericidal property against cariogenic bacteria, prevention of dentin de-mineralization, and inhibition of collagenases within the dentin collagen,[17] which were not described in the present study. The long-term effects of SDF treatment on the permeability of dentin therefore may warrant further micro-architectural investigation.

Regarding enamel hypomineralization, our study confirmed that the permeability of non-carious hypomineralized enamel is unaffected by SDF treatment. Our findings were consistent with those reported by Li et al., where silver particles *in-vitro* could penetrate through the pellicle complex, along with the rod sheaths into the demineralized enamel rods, but not sound enamel.[69] It has been shown that true mineralization of enamel caries is a very rare phenomenon *in-vivo*, because the surface of the lesion forms a diffusion barrier against uptake of minerals into the subsurface region.[60] Likewise, intact hypomineralized enamel surface without caries or cracks, while displaying superficial SDF staining, may in fact serve as a barrier against SDF.

While systematic reviews consistently supported the effectiveness of SDF in arresting coronal caries in the primary dentition and arresting and preventing root caries in adults, there is insufficient evidence to draw conclusions on SDF for prevention in primary teeth and prevention and arrest in permanent teeth in children.[19] Our present study suggested

that if the enamel surface were intact, even in teeth with severe hypomineralization, the effect of SDF is limited to the enamel surface. However, the exact effects of SDF on intact enamel surface, especially an enamel surface already treated with other biomaterials, such as fluoride varnish, remain unknown. Furthermore, knowledge of the effects of SDF on carious enamel, including those found in interproximal sites, may have profound implication on the preventive properties of SDF against dentinal caries and warrant further study. Additionally, while our study confirmed the effects of SDF on carious dentin in primary teeth, the effects of SDF on exposed dentin, carious or non-carious, in molars with hypomineralized enamel may have direct implication on the treatment of hypersensitivity in patients with MIH, and await further investigation.

In addition to SDF, topical fluoridation, casein phosphopeptide-amorphous calcium phosphate (CPP-ACP) application, and desensitizing products containing 8% arginine have been shown to reduce hypersensitivity in patients with MIH.[14] Likewise, sealing of hypersensitive MIH-affected molars with resin and glass ionomer without the use of SDF can improve hypersensitivity and oral health-related quality of life.[79,80] It may be possible to study the changes in the permeability of enamel and dentin using the present methodology under modified protocols such as curing light use immediately after SDF application, multiple applications of SDF, or under the aforementioned treatment conditions other than SDF application. However, it should be noted that the x-ray attenuation of predominantly organic materials such as non-radiopaque resin may pose difficulties during the segmentation of microCT volumes.

Correlative Elemental Mapping:

Our previous study has shown that it is possible to correlates measured MD with respective Ca^{2+}, P^{3-} and Zn^{2+} elemental levels in healthy and diseased dentin.[39,40] Comparing **Figure 6** and **Figure 9**, we illustrated that SDF-treated carious dentin, transparent dentin, and sound dentin became further distinct from their untreated counterpart when Ca^{2+}, P^{3-}, and Zn^{2+} levels were included in the analysis. Remarkably, SDF-treated carious dentin was further likened to transparent, while on the other hand, SDF-treated and untreated sound dentin that were physically similar became physiochemically distinct. We further showed that Zn^{2+}, a critical indicator of tissue inflammation and the localization thereof, is a significant effector of permeability.[40,81,82] We postulated that Zn^{2+}-mediated mineral densities and the resulting permeabilities of enamel and dentin are biologically controlled, underscoring tissue adaptation and pulp function.[82,83] In dentin caries, Zn^{2+} localization in carious and transparent dentin represents an acquired inflammatory response to pathogens, whereas in molar incisor hypomineralization, the localization of Zn^{2+} in hypomineralized enamel embodies an developmental inflammatory imprint during times of systemic stress. The high intra- and inter-tissue variations in the physicochemical properties across dentin zones and enamel of varying hypomineralization support the notion that micro-scale changes within dentin tubules and enamel rods culminate in tissue-level characteristics and eventual organ-level responses that reflect the overall disease status, whether acquired or developmental, amid protective and risk factors.[82,83]

LIMITATIONS:

In the present study, a greyscale threshold within a specified range for each tissue type was used to segment the microCT data. For carious dentin of primary teeth, the segmentation threshold was set to 9-10% of the greyscale value of sound dentin; hypomineralized enamel of permanent teeth, 51-60% of the greyscale value of normal enamel; dentin of permanent teeth, 46-48% of the of the greyscale value of adjacent sound dentin. When the MD of the tissue varies broadly, as in the case of severe enamel hypomineralization (15.1-34.6% de-mineralization compared to reference normal enamel), the range of segmentation thresholds was broadened to accurately reflect the underlying microstructures. However, structures with excessively high or low MD, such as sound enamel or severely de-mineralized dentin, could not be analyzed as these structures cannot be anatomically defined after the segmentation of microCT 3D image. Also, some volumes of hypomineralized enamel were affected by caries as indicated by greatly reduced MD, hence, not selected for computation.

Additionally, the effects of superficial layers such as smear layer or enamel remineralization also could not be analyzed using the method of present study because of truncation artifact along the edge of the microCT image. Furthermore, ring artifacts inherent in each reconstructed microCT scan required that regions with altered radiopacity not be selected for analysis. More advanced techniques using advanced filter and machine learning may both increase the accuracy and reduce the noise of the segmented data. Furthermore, the observed microarchitecture and computed permeabilities and physical properties were based predominantly on inorganic constituents of dentin and enamel due to reduced x-ray attenuation of organic materials.

Hence, the effects of organic constituents such as serum proteins, cell bodies, and salivary components on permeability could not be accounted for using present methodology.

Given the marked difference in the mean permeability of SDF-treated and untreated carious dentin, and basing the standard deviation of the permeability on SDF-treated carious dentin, our study met the anticipated sample size (SDF-treated: N>2; untreated: N>2) to have sufficient statistical power to detect the effect of SDF treatment. However, a larger sample size including both carious primary teeth and hypomineralized permanent teeth may provide additional physicochemical insights differentiating the effects of anatomic locations, patient demographics, other restorative and preventive treatments, and related genetic and environmental conditions.

CONCLUSION:

The present study illustrated a novel method to analyze the effects of biomaterials on tissue mineralization and revealed the following:

1. Progression of caries is spatially and chemically dynamic.
2. The physicochemical properties of SDF-treated carious dentin are likened to transparent dentin.
3. Inflammation-mediated Zn^{2+} localization can alter dentin and enamel permeability.
4. The permeability of hypomineralized enamel is comparable to sound dentin.

5. Permeability of non-carious hypomineralized enamel is unaffected by SDF treatment.

Permeability properties of dentin determine its sensitivity and the degree of pulpal response to restorative procedure materials and microleakage. The prospect of employing biologic factors to permeate across dentin to modify the formation of intratubular and/or tertiary dentin, thereby lower dentin permeability and protecting the pulp, has been speculated for decades.[2] Here, we confirmed inducible changes in the physicochemical properties, including permeability, of carious dentin after SDF treatment. Silver diamine fluoride treatment alters physicochemical properties of carious dentin but not hypomineralized enamel, and reduces the permeability of carious dentin, not transparent dentin. Using the present methodology, novel formulations of SDF such as one containing potassium iodide,[84] or materials such as bioglass or silver nanoparticles, [34,85] can likewise be analyzed.

Everyday clinical and radiographic diagnosis of caries and enamel hypomineralization remains disjunct from a patho-biological principle reflecting the disease process. Here, we demonstrated inflammatory Zn^{2+}-mediated mineral densities that resulted in altered permeabilities of enamel and dentin. These observations were postulated to be biologically controlled and underscored tissue adaptation and pulp function.[82,83] The physiochemically dynamic nature of caries lesion progression endorsed the classification of caries based on activity status. Novel diagnostic methods, such as the use of florescence imaging to differentiate active versus inactive lesion, the use of near-

infrared imaging for detection of early carious lesion,[86,87] or molecular diagnostic adjuncts to pulpal health,[88] may represent only the beginning a personalized, biologic approach to diagnosing and treating beyond the deceivingly physical aspects of pathological dental tissues.

REFERENCES:

1. Pashley, D. H. Dynamics of the Pulpo-Dentin Complex. *Critical Reviews in Oral Biology & Medicine* **7**, 104–133 (1996).
2. Pashley, D. H., Pashley, E. L., Carvalho, R. M. & Tay, F. R. The effects of dentin permeability on restorative dentistry. *Dent Clin North Am* **46**, 211–245 (2002).
3. Greenhill, J. D. & Pashley, D. H. *The Effects of Desensitizing Agents on the Hydraulic Conductance of Human Dentin in vitro*. *J Dent Res* vol. 60 (1981).
4. Pitts, N. B. *et al.* Dental caries. *Nat Rev Dis Primers* **3**, (2017).
5. Fleming, E. & Afful, J. Prevalence of Total and Untreated Dental Caries Among Youth: United States, 2015-2016. *NCHS Data Brief* 1–8 (2018).
6. Frank, R. M. *Structural Events in the Caries Process in Enamel, Cementum, and Dentin*. *J Dent Res* vol. 69 (1990).
7. Mjör, I. A. Dentin permeability: the basis for understanding pulp reactions and adhesive technology. *Braz Dent J* **20**, 3–16 (2009).
8. Pashley, E. L., Talman, R., Horner, J. A. & Pashley, D. H. Permeability of normal versus carious dentin. *Dental Traumatology* **7**, 207–211 (1991).
9. Tagami, J., Hosoda, H., Burrow, M. F. & Nakajima, M. Effect of aging and caries on dentin permeability. *Proc Finn Dent Soc* **88 Suppl 1**, 149–54 (1992).
10. Somani, C. *et al.* An update of treatment modalities in children and adolescents with teeth affected by molar incisor hypomineralisation (MIH): a systematic review. *European Archives of Paediatric Dentistry* vol. 23 39–64 Preprint at https://doi.org/10.1007/s40368-021-00635-0 (2022).

11. Wright, J. T. Diagnosis and Management of Molar–Incisor Hypomineralization. in *Handbook of Clinical Techniques in Pediatric Dentistry* 131–141 (Wiley, 2021). doi:10.1002/9781119661085.ch11.

12. Mahoney, E. K. & Farah, R. Molar Incisor Hypomineralization: Structure, Composition, and Properties. in *Planning and Care for Children and Adolescents with Dental Enamel Defects: Etiology, Research and Contemporary Management* 73–84 (Springer Berlin Heidelberg, 2015). doi:10.1007/978-3-662-44800-7_6.

13. Crombie, F. A. *et al.* Characterisation of developmentally hypomineralised human enamel. *J Dent* **41**, 611–618 (2013).

14. Linner, T. *et al.* Hypersensitivity in teeth affected by molar-incisor hypomineralization (MIH). *Sci Rep* **11**, (2021).

15. Xie, Z. H., Mahoney, E. K., Kilpatrick, N. M., Swain, M. V. & Hoffman, M. On the structure-property relationship of sound and hypomineralized enamel. *Acta Biomater* **3**, 865–872 (2007).

16. Chibinski, A. C. *et al.* Silver Diamine Fluoride Has Efficacy in Controlling Caries Progression in Primary Teeth: A Systematic Review and Meta-Analysis. *Caries Research* vol. 51 527–541 Preprint at https://doi.org/10.1159/000478668 (2017).

17. Zhao, I. S. *et al.* Mechanisms of silver diamine fluoride on arresting caries: a literature review. *International Dental Journal* vol. 68 67–76 Preprint at https://doi.org/10.1111/idj.12320 (2018).

18. Oliveira, B. H., Rajendra, A., Veitz-Keenan, A. & Niederman, R. The effect of silver diamine fluoride in preventing caries in the primary dentition: A systematic review and meta-analysis. *Caries Res* **53**, 24–32 (2019).

19. Seifo, N., Cassie, H., Radford, J. R. & Innes, N. P. T. Silver diamine fluoride for managing carious lesions: An umbrella review. *BMC Oral Health* vol. 19 Preprint at https://doi.org/10.1186/s12903-019-0830-5 (2019).

20. Seifo, N. *et al.* The use of silver diamine fluoride (SDF) in dental practice. *Br Dent J* **228**, 75–81 (2020).

21. Mei, M. L. *et al.* Formation of Fluorohydroxyapatite with Silver Diamine Fluoride. *J Dent Res* **96**, 1122–1128 (2017).

22. Mei, M. L., Lo, E. C. M. & Chu, C. H. Arresting Dentine Caries with Silver Diamine Fluoride: What's Behind It? *Journal of Dental Research* vol. 97 751–758 Preprint at https://doi.org/10.1177/0022034518774783 (2018).

23. Mei, M. L. *et al.* Inhibitory effect of silver diamine fluoride on dentine demineralisation and collagen degradation. *J Dent* **41**, 809–817 (2013).

24. MacLean, J. Minimally Invasive Treatment for Molar-Incisor Hypomineralization. *Decisions in Dentistry* **4**, 18–23 (2018).

25. Castillo, J. L. *et al.* The short-term effects of diammine silver fluoride on tooth sensitivity: A randomized controlled trial. *J Dent Res* **90**, 203–208 (2011).

26. Ballikaya, E., Ünverdi, G. E. & Cehreli, Z. C. Management of initial carious lesions of hypomineralized molars (MIH) with silver diamine fluoride or silver-modified atraumatic restorative treatment (SMART): 1-year results of a prospective, randomized clinical trial. *Clin Oral Investig* **26**, 2197–2205 (2022).

27. Rauen, C. A. *et al.* Effect of bleaching agents containing fluoride or calcium on enamel microhardness, roughness and permeability. *Braz J Oral Sci* **14**, 262–266 (2015).

28. Zero, D. T., Rahbek, I., Fu, J., Proskin, H. M. & Featherstone, J. D. B. Comparison of the Iodide Permeability Test, the Surface Microhardness Test, and Mineral Dissolution of Bovine Enamel following Acid Challenge. *Caries Res* **24**, 181–188 (1990).

29. Bertacci, A., Chersoni, S., Davidson, C. L. & Prati, C. In vivo enamel fluid movement. *Eur J Oral Sci* **115**, 169–173 (2007).

30. Lucchese, A., Bertacci, A., Chersoni, S. & Portelli, M. *Primary enamel permeability: a SEM evaluation in vivo*. *Article in European Journal of Paediatric Dentistry* https://www.researchgate.net/publication/230840939 (2012).

31. Pashley, D. H., Nelson, R. & Kepler, E. E. The Effects of Plasma and Salivary Constituents on Dentin Permeability. *J Dent Res* **61**, 978–981 (1982).

32. Koutsi, V. *et al.* The effect of dentin depth on the permeability and ultrastructure of primary molars. *Pediatr Dent* **16**, 29–35 (1994).

33. Hiller, K. A., Buchalla, W., Grillmeier, I., Neubauer, C. & Schmalz, G. In vitro effects of hydroxyapatite containing toothpastes on dentin permeability after multiple applications and ageing. *Sci Rep* **8**, (2018).

34. Dias, F. A., Vidal, C. M. P., Comnick, C. L., Xie, X. J. & Berger, S. B. Effect of silver nanoparticles associated with fluoride on the progression of root dentin caries in vitro. *PLoS One* **18**, (2023).

35. Abdelaziz, M. *et al.* Monitoring silver diamine fluoride application with optical coherence tomography and thermal imaging: An in vitro proof of concept study. *Lasers Surg Med* **54**, 790–803 (2022).

36. Jud, C. *et al.* Dentinal tubules revealed with X-ray tensor tomography. *Dental Materials* **32**, 1189–1195 (2016).

37. Chairside Guide: Silver Diamine Fluoride in the Management of Dental Caries Lesions. *The Reference Manual of Pediatric Dentistry* 612–613 (2022).

38. Burwell, A. K. *et al.* Functional remineralization of dentin lesions using polymer-induced liquid-precursor process. *PLoS One* **7**, (2012).

39. Sulyanto, R. M. *et al.* Biomineralization of Dental Tissues Treated with Silver Diamine Fluoride. *J Dent Res* **100**, 1099–1108 (2021).

40. Djomehri, S. I. *et al.* Mineral density volume gradients in normal and diseased human tissues. *PLoS One* **10**, (2015).

41. Ferguson, J. C. *et al.* Update 3.0 to “PuMA: The Porous Microstructure Analysis software”, (PII:S2352711018300281). *SoftwareX* **15**, 100775 (2021).

42. Domander, R., Felder, A. A. & Doube, M. BoneJ2 - refactoring established research software. *Wellcome Open Res* **6**, 37 (2021).

43. Schneider, C. A., Rasband, W. S. & Eliceiri, K. W. NIH Image to ImageJ: 25 years of image analysis. *Nat Methods* **9**, 671–675 (2012).

44. Vianna, R. S., Cunha, A. M., Azeredo, R. B. V., Leiderman, R. & Pereira, A. Computing effective permeability of porous media with FEM and Micro-CT: An educational approach. *Fluids* **5**, (2020).

45. Odgaard, A. Three-dimensional methods for quantification of cancellous bone architecture. *Bone* **20**, 315–328 (1997).

46. Dougherty, R. & Kunzelmann, K.-H. Computing Local Thickness of 3D Structures with ImageJ. *Microscopy and Microanalysis* **13**, (2007).

47. Ayachit, U. *et al.* Catalyst Revised: Rethinking the ParaView in Situ Analysis and Visualization API. in 484–494 (2021). doi:10.1007/978-3-030-90539-2_33.

48. GraphPad Software. GraphPad Prism version 9.4.1 for Windows. Preprint at www.graphpad.com.

49. RStudio Team. RStudio: Integrated Development for R. Preprint at http://www.rstudio.com/ (2020).

50. Wickham, H. & Bryan, J. readxl: Read Excel Files. Preprint at https://CRAN.R-project.org/package=readxl (2022).

51. Wickham, H., François, R., Henry, L. & Müller, K. dplyr: A Grammar of Data Manipulation. Preprint at https://CRAN.R-project.org/package=dplyr (2022).

52. Oksanen, J. & Simpson, G. L. vegan: Community Ecology Package. Preprint at https://CRAN.R-project.org/package=vegan (2022).

53. Gaujoux, R. & Seoighe, C. A flexible R package for nonnegative matrix factorization. *BMC Bioinformatics* **11**, 367 (2010).

54. Martinez Arbizu, P. pairwiseAdonis: Pairwise Multilevel Comparison using Adonis. Preprint at (2020).

55. Adler, D., Kelly, S. T., Elliott, T. & Adamson, J. vioplot: violin plot. Preprint at (2022).

56. Hadley Wickham. *ggplot2: Elegant Graphics for Data Analysis*. (Springer-Verlag New York, 2016).

57. Yamada, T., Nakamura, K., Iwaku, M. & Fusayama, T. The Extent of the Odontoblast Process in Normal and Carious Human Dentin. *J Dent Res* **62**, 798–802 (1983).

58. Ogawa, K., Yamashita, Y., Ichijo, T. & Fusayama, T. The Ultrastructure and Hardness of the Transparent of Human Carious Dentin. *J Dent Res* **62**, 7–10 (1983).

59. Holland, G. R. *The Odontoblast Process: Form and Function*. (1985).

60. Nyvad, B. & Fejerskov, O. Assessing the stage of caries lesion activity on the basis of clinical and microbiological examination. *Community Dent Oral Epidemiol* **25**, 69–75 (1997).

61. Sarnat, H. & Massler, M. Microstructure of Active and Arrested Dentinal Caries. *J Dent Res* **44**, 1389–1401 (1965).

62. Drancourt, N. *et al.* Carious lesion activity assessment in clinical practice: a systematic review. *Clinical Oral Investigations* vol. 23 1513–1524 Preprint at https://doi.org/10.1007/s00784-019-02839-7 (2019).

63. Nyvad, B., Machiulskiene, V. & Baelum, V. Construct and Predictive Validity of Clinical Caries Diagnostic Criteria Assessing Lesion Activity. *J Dent Res* **82**, 117–122 (2003).

64. Nyvad, B., Machiulskiene, V. & Baelum, V. Reliability of a New Caries Diagnostic System Differentiating between Active and Inactive Caries Lesions. *Caries Res* **33**, 252–260 (1999).

65. Maltz, M. *et al.* Can We Diagnose a Patient's Caries Activity Based on Lesion Activity Assessment? Findings from a Cohort Study. *Caries Res* **54**, 218–225 (2020).

66. Rup, A. G. *et al.* Classification of a patient's caries activity based on lesion activity assessment among adults: findings from a prospective cohort study. *Clin Oral Investig* (2022) doi:10.1007/s00784-022-04702-8.

67. Santamaría, R. M. *et al.* How to Intervene in the Caries Process: Dentin Caries in Primary Teeth. *Caries Research* vol. 54 306–323 Preprint at https://doi.org/10.1159/000508899 (2020).

68. Elhennawy, K. *et al.* Selective vs stepwise removal of deep carious lesions in primary molars: 24 months follow-up from a randomized controlled trial. *Clin Oral Investig* **25**, 645–652 (2021).

69. Li, Y. *et al.* Assessment of the Silver Penetration and Distribution in Carious Lesions of Deciduous Teeth Treated with Silver Diamine Fluoride. *Caries Res* **53**, 431–440 (2019).

70. Ge, J., Cui, F. Z., Wang, X. M. & Feng, H. L. Property variations in the prism and the organic sheath within enamel by nanoindentation. *Biomaterials* **26**, 3333–3339 (2005).

71. Melin, L. *et al.* XRMA and ToF-SIMS Analysis of Normal and Hypomineralized Enamel. *Microscopy and Microanalysis* **21**, 407–421 (2015).

72. Petrova, S., Tomov, G., Shindova, M. & Belcheva, A. Phenotypic characteristics of molar-incisor mineralization-affected teeth. A light and

scanning electron microscopy study. *Biotechnology and Biotechnological Equipment* **35**, 1906–1911 (2021).

73. Jälevik, B., Dietz, W. & Norén, J. G. *Scanning electron micrograph analysis of hypomineralized enamel in permanent first molars*. *International Journal of Paediatric Dentistry* vol. 15 (2005).

74. Cardoso-Martins, I., Pessanha, S., Coelho, A., Arantes-Oliveira, S. & Marques, P. F. Evaluation of the Efficacy of CPP-ACP Remineralizing Mousse in Molar-Incisor Hypomineralized Teeth Using Polarized Raman and Scanning Electron Microscopy—An In Vitro Study. *Biomedicines* **10**, (2022).

75. Fagrell, T. G., Dietz, W., Jälevik, B. & Norén, J. G. Chemical, mechanical and morphological properties of hypomineralized enamel of permanent first molars. *Acta Odontol Scand* **68**, 215–222 (2010).

76. Fagrell, T. G., Lingström, P., Olsson, S., Steiniger, F. & Norén, J. G. Bacterial invasion of dentinal tubules beneath apparently intact but hypomineralized enamel in molar teeth with molar incisor hypomineralization. *Int J Paediatr Dent* **18**, 333–340 (2008).

77. Xie, Z., Kilpatrick, N. M., Swain, M. V., Munroe, P. R. & Hoffman, M. Transmission electron microscope characterisation of molar-incisor-hypomineralisation. *J Mater Sci Mater Med* **19**, 3187–3192 (2008).

78. Heijs, S. C. B., Dietz, W., Norén, J. G., Blanksma, N. G. & Jälevik, B. Morphology and chemical composition of dentin in permanent first molars with the diagnose MIH. *Swed Dent J* **31**, 155–64 (2007).

79. Diago, A. M. Dello *et al.* Hypersensitivity in molar incisor hypomineralization: Superficial infiltration treatment. *Applied Sciences (Switzerland)* **11**, 1–7 (2021).

80. Bekes, K. *et al.* Changes in oral health-related quality of life after treatment of hypersensitive molar incisor hypomineralization–affected molars with a sealing. *Clin Oral Investig* **25**, 6449–6454 (2021).

81. Rahman, M. T., Hossain, A., Pin, C. H. & Yahya, N. A. Zinc and Metallothionein in the Development and Progression of Dental Caries. *Biol Trace Elem Res* **187**, 51–58 (2019).

82. Ho, S. P. *et al.* Architecture-Guided Fluid Flow Directs Renal Biomineralization. *Sci Rep* **8**, 14157 (2018).

83. He, R. *et al.* Insights Into Pulp Biomineralization in Human Teeth. *Frontiers in Dental Medicine* **3**, (2022).

84. Lee, K. E., Erdenebulgan, M., Kang, C. M., Jung, H. I. & Song, J. S. Effect of Silver Diamine Fluoride and Potassium Iodide Solution on Enamel Remineralization and Discoloration in Artificial Caries. *Materials* **15**, (2022).

85. Bang, S. J. *et al.* Characterization of Physical and Biological Properties of a Caries-Arresting Liquid Containing Copper Doped Bioglass Nanoparticles. *Pharmaceutics* **14**, (2022).

86. Bounds, A. D. & Girkin, J. M. Early stage dental caries detection using near infrared spatial frequency domain imaging. *Sci Rep* **11**, (2021).

87. Park, S. W. *et al.* Lesion activity assessment of early caries using dye-enhanced quantitative light-induced fluorescence. *Sci Rep* **12**, (2022).

88. El karim, I. A. *et al.* Deciphering Reparative Processes in the Inflamed Dental Pulp. *Frontiers in Dental Medicine* **2**, (2021).

Publishing Agreement

It is the policy of the University to encourage open access and broad distribution of all theses, dissertations, and manuscripts. The Graduate Division will facilitate the distribution of UCSF theses, dissertations, and manuscripts to the UCSF Library for open access and distribution. UCSF will make such theses, dissertations, and manuscripts accessible to the public and will take reasonable steps to preserve these works in perpetuity.

I hereby grant the non-exclusive, perpetual right to The Regents of the University of California to reproduce, publicly display, distribute, preserve, and publish copies of my thesis, dissertation, or manuscript in any form or media, now existing or later derived, including access online for teaching, research, and public service purposes.

DocuSigned by:
Conrad Chou
5BD7D6DFCDF645A...
Author Signature

5/31/2023
Date